Crystal structure and modeling of the tetrahedral intermediate state of methylmalonate-semialdehyde dehydrogenase (MMSDH) from *Oceanimonas doudoroffii*[§]

Hackwon Do[1]**, Chang Woo Lee**[1,2]**,**
Sung Gu Lee[1,2]**, Hara Kang**[3]**, Chul Min Park**[4]**,**
Hak Jun Kim[5]**, Hyun Park**[1,2*]**, HaJeung Park**[6*]**,**
and Jun Hyuck Lee[1,2*]

[1]*Division of Polar Life Sciences, Korea Polar Research Institute, Incheon 406-840, Republic of Korea*
[2]*Department of Polar Sciences, University of Science and Technology, Incheon 406-840, Republic of Korea*
[3]*Division of Life Science, College of Life Science and Bioengineering, Incheon National University, Incheon 406-772, Republic of Korea*
[4]*Medicinal Chemistry Research Center, Bio-Organic Division, Korea Research Institute of Chemical Technology, Daejeon 305-600, Republic of Korea*
[5]*Department of Chemistry, Pukyong National University, Busan 608-739, Republic of Korea*
[6]*X-Ray Core, The Scripps Research Institute, Scripps Florida, 130 Scripps Way #1A1, Jupiter, FL 33458, USA*

The gene product of *dddC* (Uniprot code G5CZI2), from the Gram-negative marine bacterium *Oceanimonas doudoroffii*, is a methylmalonate-semialdehyde dehydrogenase (*Odo*MMSDH) enzyme. MMSDH is a member of the aldehyde dehydrogenase superfamily, and it catalyzes the NAD-dependent decarboxylation of methylmalonate semialdehyde to propionyl-CoA. We determined the crystal structure of *Odo*MMSDH at 2.9 Å resolution. Among the twelve molecules in the asymmetric unit, six subunits complexed with NAD, which was carried along the protein purification steps. *Odo*MMSDH exists as a stable homodimer in solution; each subunit consists of three distinct domains: an NAD-binding domain, a catalytic domain, and an oligomerization domain. Computational modeling studies of the *Odo*MMSDH structure revealed key residues important for substrate recognition and tetrahedral intermediate stabilization. Two basic residues (Arg103 and Arg279) and six hydrophobic residues (Phe150, Met153, Val154, Trp157, Met281, and Phe449) were found to be important for tetrahedral intermediate binding. Modeling data also suggested that the backbone amide of Cys280 and the side chain amine of Asn149 function as the oxyanion hole during the enzymatic reaction. Our results provide useful insights into the substrate recognition site residues and catalytic mechanism of *Odo*MMSDH.

Introduction

Dimethylsulfoniopropionate (DMSP) is a metabolite that is primarily produced by marine phytoplankton, and is a main source of carbon and sulfur for marine microbes (Reisch *et al.*, 2011). In addition, DMSP is the precursor of the climatically important dimethyl sulfide (DMS) gas, a volatile sulfur compound that plays a role in cloud condensation nuclei formation (Stefels, 2000; Sunda *et al.*, 2002). Degradation of DMSP by marine bacteria occurs via two competing pathways, including the DMSP cleavage pathway and the DMSP demethylation pathway. In the DMSP cleavage pathway, DMSP lyases (DddD, DddL, DddP, DddQ, DddW, and DddY) act on the metabolites to yield DMS and acrylate. Acrylate is further degraded by DddA and DddC (Curson *et al.*, 2011a, 2012; Reisch *et al.*, 2011; Todd *et al.*, 2011). In the DMSP demethylation pathway, DMSP demethylases (DmdA, DmdB, DmdC, and DmdD) convert DMSP into methyl 3-mercaptoproprionate, using tetrahydrofolate as the methyl acceptor (Todd *et al.*, 2010; Curson *et al.*, 2011b, 2012; Reisch *et al.*, 2011; Todd *et al.*, 2012).

The newly classified gammaproteobacterium *Oceanimonas doudoroffii* (ATCC 27123) was isolated from seawater and was shown to contain multiple DMSP lyase genes. *dddC* is located near the DMSP lyase genes and encodes methylmalonate-semialdehyde dehydrogenase (MMSDH) (Curson *et al.*, 2012). MMSDH belongs to the coenzyme A-dependent aldehyde dehydrogenase (ALDH) subfamily and is involved in the decarboxylation of methylmalonate-semialdehyde (MMSA) downstream of the DMSP cleavage pathway (Todd *et al.*, 2010).

ALDH has been identified and characterized in many species ranging from bacteria to humans. Phylogenetic trees based on sequences from the ALDHs and a broad range of substrates indicate that the ALDH family evolved from a common ancestral gene by separation (Vasiliou and Nebert, 2005). ALDHs catalyze the oxidation of aldehydes into acidic compounds via two separate acylation and deacylation steps. The acylation step involves nucleophilic attack of the catalytic cysteine residue with the NAD cofactor, leading to the

formation of a thioacyl enzyme intermediate and NADH. Next, the acyl-enzyme intermediate undergoes nucleophilic attack by either a water or CoA to produce the final product, propionyl-coenzyme A. All ALDHs exist either as a homodimer or as a homotetramer. The human liver ALDH1 (tetramer), bovine liver ALDH2 (tetramer), cod liver ALDH9 (tetramer), and rat liver ALDH3 (dimer) have been studied extensively (Liu *et al.*, 1997; Steinmetz *et al.*, 1997; Johansson *et al.*, 1998). The tetramer forms through dimer-dimer interaction and the dimer structure of rat liver ALDH3 can be superimposed on the tetramer structures of ALDH1, ALDH2, and ALDH9. Thus, the dimer interaction is highly conserved in ALDH classes while the tetramer interaction is not. In addition, ALDHs can be classified into two groups depending on the deacylation mechanism: the CoA-dependent group and the CoA-independent group, which uses a water molecule as the nucleophile. Additionally, CoA-dependent ALDHs exhibit a ping-pong mechanism, wherein the release of NADH occurs before CoA binding. MMSDH is a member of the CoA-dependent ALDH gene family and catalyzes the oxidative decarboxylation of MMSA to propionyl-coenzyme A (Bannerjee *et al.*, 1970; Steele *et al.*, 1992; Hempel *et al.*, 1993; Zhang *et al.*, 1996; Vasiliou and Nebert, 2005; Stines-Chaumeil *et al.*, 2006). Recently, the NAD-bound structure of MMSDH from *Bacillus subtilis* (*Bsu*MMSDH) was determined in the tetramer form; it was suggested that the highly conserved Arg124 and Arg301 residues of *Bsu*MMSDH are essential for MMSA binding via direct interactions with the carboxylate group (Talfournier *et al.*, 2011; Bchini *et al.*, 2012). To better understand the enzymatic mechanisms of MMSDH from *Oceanimonas doudoroffii* (*Odo*MMSDH), we determined the crystal structure of *Odo*MMSDH. During the protein purification step, the protein was estimated to be a stable dimer in solution, suggesting that the oligomerization of *Odo*MMSDH differs from that of *Bsu*MMSDH. Moreover, the determined *Odo*MMSDH structure, together with molecular modeling studies of the reaction intermediate of the substrate, outlines the substrate binding modes and provides information regarding the manner in which the enzyme binds to the substrate and catalyzes decarboxylation.

Materials and Methods

Expression and purification of recombinant OdoMMSDH

Codon optimization was used to synthesize the full-length *dddC* encoding MMSDH (498 amino acids; 54 kDa) from *Oceanimonas doudoroffii* for expression in *Escherichia coli*. To produce a thrombin-cleavable, N-terminal 6-His-tagged recombinant protein, chemically synthesized *dddC* (Bioneer Inc.) containing *Nde*I and *Xho*I restriction sites was inserted into the pET28a vector. Following thrombin cleavage, the final purified construct contained an additional GSH sequence at its N-terminus. Expression of the construct in *E. coli* BL21(DE3) was induced by application of 1 mM isopropyl-β-D-1-thiogalactopyranoside at 25°C for 20 h. The cell pellet was harvested by centrifugation and resuspended in cold lysis buffer containing 50 mM sodium phosphate (pH 8.0), 300 mM NaCl, 5 mM imidazole, 0.5 mg/ml lysozyme, and 1 mM phenylmethylsulfonyl fluoride. The cells were

disrupted by ultrasonication (Vibra-Cell VCX400; Sonics & Materials, Inc.) for 10 min (5-sec pulse on/off) at 35% amplitude of maximum power. The cell lysate was centrifuged at 17,000 rpm for 40 min at 4°C, and the supernatant containing *Odo*MMSDH was collected. The first purification step involved typical His-tag affinity purification, wherein Ni-NTA beads (5 ml) bound to *Odo*MMSDH were washed with 10 column-volumes of washing buffer (50 mM sodium phosphate; pH 8.0, 300 mM NaCl, and 20 mM imidazole), and eluted (30 ml of each fraction) with elution buffer (washing buffer containing 300 mM imidazole). After thrombin cleavage of the 6-His-tag overnight at 4°C, size-exclusion chromatography was performed. The sample was filtered using a 0.22-μm syringe filter and applied to a HiLoad 16/60 Superdex 200 column (GE Healthcare) that was pre-equilibrated with 20 mM Tris-HCl (pH 8.0), 150 mM NaCl, and 1 mM DTT. Purified *Odo*MMSDH was concentrated to 32.2 mg/ml and used for crystallization experiments. The concentration of *Odo*MMSDH was determined using UV spectrophotometry at 280 nm, applying an extinction coefficient of 44,265 $M^{-1} \cdot cm^{-1}$ based on the amino acid sequence.

Analytical size exclusion chromatography

To estimate the oligomeric state of *Odo*MMSDH, the purified protein sample was evaluated by size exclusion on a Superdex 200 (26/60) column equilibrated with 150 mM NaCl and 20 mM HEPES, pH 7.4, at a flow rate of 1 ml/min. The molecular weight of OdoMMSDH was estimated based on a standard curve generated using the elution profiles of standard proteins with known molecular weights. The elution

Table 1. Data collection and refinement statistics

Data set	*Odo*MMSDH+NAD
Space group	$P2_12_12$
Wavelength (Å)	1.5418
Resolution range (Å)	49.66–2.90 (3.06–2.90)
No. of observed reflections	788310 (120407)
No. of unique reflections	132599 (19154)
R_{sym} [a] (%)	13.4 (37.7)
Average I/σ	10.2 (4.2)
Completeness (%)	99.4 (99.5)
Multiplicity	5.9 (6.3)
Refinement	
Resolution (Å)	50–2.9 (2.98–2.90)
No. of residues	5,851 /six dimers
No. of NAD molecules	6
No. of water molecules	709
R_{cryst} [b] total (%)	19.0 (27.3)
R_{free} [c] total (%)	24.5 (34.6)
R.m.s. bond length (Å)	0.011
R.m.s. bond angle (°)	1.36
Average B value ($Å^2$) (protein)	33.7
Average B value ($Å^2$) (NADs)	40.8
Average B value ($Å^2$) (solvent)	17.9

[a] $R_{sym} = \Sigma \mid <I> - I \mid / \Sigma <I>$.
[b] $R_{cryst} = \Sigma \mid |Fo| - |Fc| \mid / \Sigma |Fo|$.
[c] R_{free} calculated with 10% of all reflections excluded from refinement stages using high resolution data.
Values in parentheses refer to the highest resolution shells.

volume of OdoMMSDH was 181.3 ml and the calculated apparent molecular weight was 110 kDa.

Crystallization and data collection

Initial crystallization screening was performed using the MCSG Suite I-IV and the Qiagen Classic Suite II (Hilden) with the sitting drop vapor diffusion method at 20°C. Initial conditions were optimized by varying the precipitant and salt concentrations. In addition, the drop volume was increased from 0.8 μl to 1 μl to generate larger crystals. Diffraction-quality crystals were obtained after two days in a drop containing 1 μl of protein solution (32.2 mg/ml protein in 20 mM Tris-HCl; pH 8.0, 150 mM NaCl, and 1 mM DTT) and 1 μl of reservoir solution (21% PEG 3350 and 0.2 M potassium

sodium tartrate; pH 7.5). Data collection was performed after flash-freezing using *n*-paratone oil as a cryoprotectant. X-ray diffraction data for the *Odo*MMSDH crystals were collected at the Korean Basic Science Institute (Ochang, South Korea) using a Rigaku MicroMax-007 HF X-ray generator. The data were indexed and integrated using iMOSFLM (Battye *et al.*, 2011). Space group determination and data scaling to a resolution of 2.9 Å was performed using POINTLESS and SCALA in the iMOSFLM graphical user interface. Scaled data were truncated using the CCP4i package (Winn *et al.*, 2011).

Structure determination
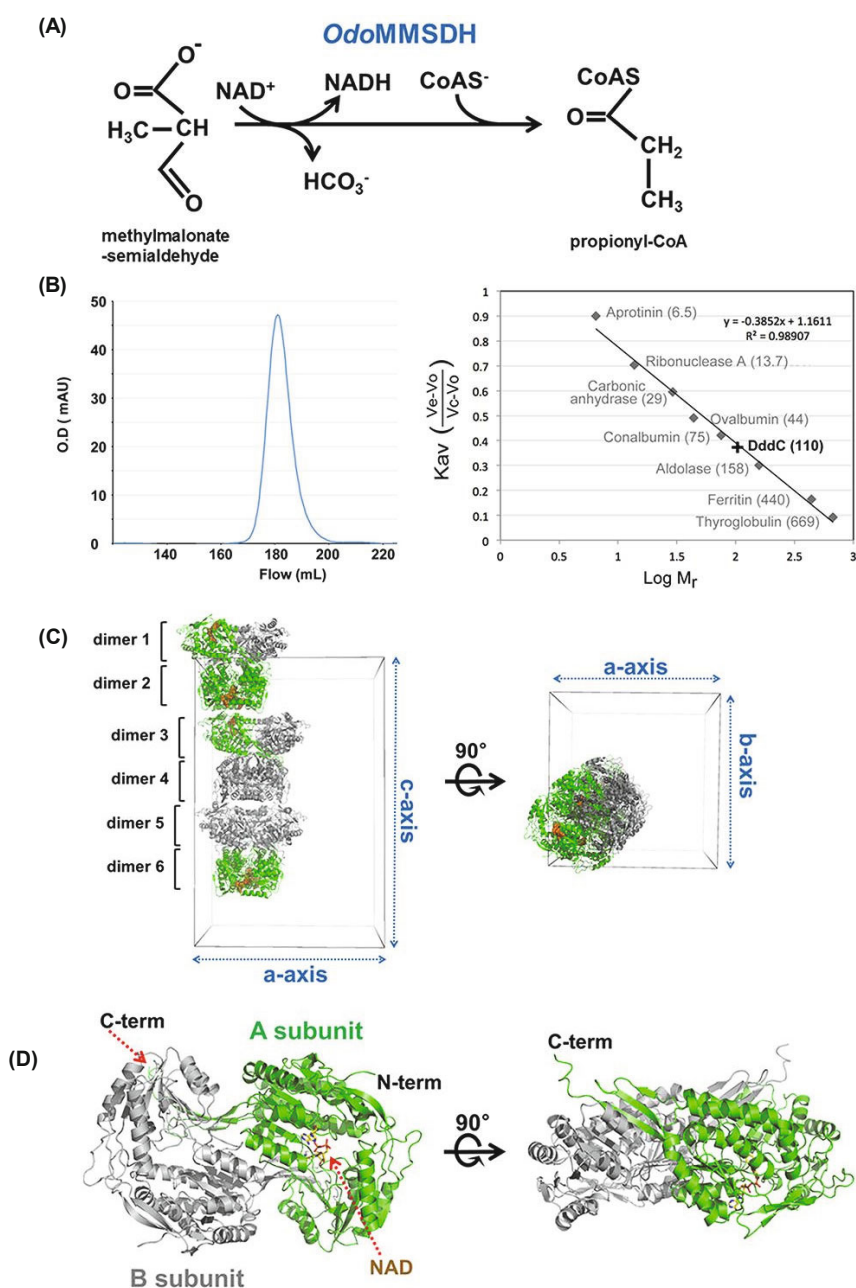
Molecular replacement was conducted using the MMSDH

Fig. 1. (A) Proposed reaction mechanism of the *Odo*MMSDH, modified from Ref. Curson *et al.* (2011a). (B) Analytical size exclusion chromatography of *Odo*MMSDH (residues 1–498; calculated molecular weight of 54.0 kDa for the polypeptide chain) showed that *Odo*MMSDH exists as a dimer in solution. Chromatograms of *Odo*MMSDH, eluting at 181.3 ml and corresponding to an apparent molecular weight of 110 kDa, and standards are shown. The numbers in parentheses show the actual molecular weights of proteins. Ve, Vo, and Vc represent elution volume, void volume (105 ml), and column volume (318.5 ml), respectively. (C) The asymmetric unit consisting of 12 *Odo*MMSDH molecules (six dimers) is shown. The unit cell is indicated by solid lines. The NAD molecules are shown as orange spheres and NAD-bound subunits are shown in green. (D) Dimeric assembly of *Odo*MMSDH. Green and gray subunits form one dimer pair (subunits A and B, respectively). The NAD molecule is bound to only subunit A. Thus, NAD interacts with individual *Odo*MMSDH subunits with different binding affinities.

dimer model from *Sinorhizobium meliloti* 1021 (PDB code: 4E4G) (Malashkevich *et al.*, unpublished data), since this molecule shares 52% sequence identity with *Odo*MMSDH. A molecular replacement solution was successfully obtained using the MOLREP program (Vagin and Teplyakov, 1997). The cross-rotation function for this model was calculated using the data in the resolution range of 30–3 Å, and the first six peaks in the output appeared as distinct solutions. The

rotation function for each solution was used to calculate a translation function, and the first six peaks yielded more distinct solutions in the translation calculations. The six dimers were sequentially located and integrated into a single PDB file. The resulting PDB file was manually adjusted using COOT and refined against the original data set using REFMAC5 (Emsley and Cowtan, 2004; Murshudov *et al.*, 2011) and Phenix (Adams *et al.*, 2002). For Phenix refine-
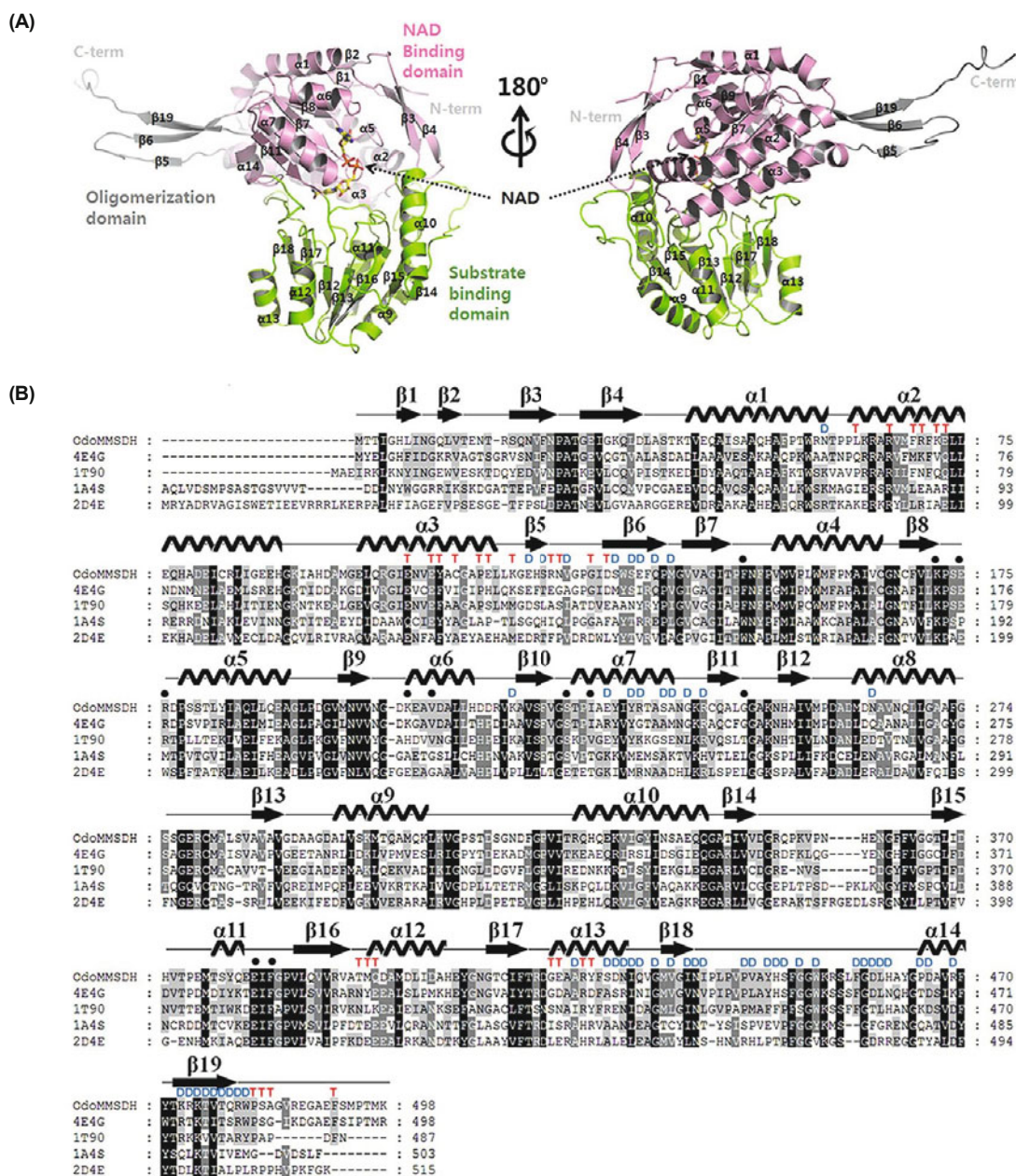

Fig. 2. Structure of *Odo*MMSDH and its sequence comparison with other MMSDHs. (A) Ribbon diagram showing overall structure of *Odo*MMSDH. The monomer structure of *Odo*MMSDH contains three domains: the NAD binding domain, the substrate-binding domain, and the oligomerization domain. The oligomerization domain (β5, β6, and β19) spanned other subunits to form a dimer. (B) Multiple sequence alignment of *Odo*MMSDH, *Sme*MMSDH (MMSDH from *Sinorhizobium meliloti* 1021; PDB code: 4E4G), *Bsu*MMSDH (PDB code: 1T90), betaine aldehyde dehydrogenase from cod liver (PDB code: 1A4S), and 5-carboxymethyl-2-hydroxymuconate semialdehyde dehydrogenase from *Thermus thermophilus* HB8 (PDB code: 2D4E) using CLUSTAL X. The residues (F148, K172, E175, R176, K205, V208, S225, I228, G247, E382, and F384) forming the NAD-binding site are indicated by filled circles. Residues participating in dimer or tetramer interactions of *Bsu*MMSDH are indicated by a blue "D" and a red "T", respectively.

ment, the ExCoR strategy was employed to improve the R_{work} and R_{free} gap (Nwachukwu *et al.*, 2013). Several monomers showed positive density around the cofactor binding site in which NADs, which were co-purified with the enzyme, were modeled. The structure was further refined after the occupancy term for the NADs were included. Refined NAD occupancies were between 0 and 100%, and NADs with 0% occupancies were deleted from the monomers. As a result, our final structure contained only six NAD molecules with 100% occupancies.

The final model showed R_{work} and R_{free} values of 19.0% and 24.5%, respectively, with 45694 atoms including 5851 amino acids, 6 NADs, and 709 water molecules (100% occupancies). Model quality was analyzed using MolProbity and PROCHECK (Laskowski *et al.*, 1993; Chen *et al.*, 2009) (Table 1). The coordinates and structure factors for the final model were deposited in the PDB under code 4ZZ7.

Modeling

A monomer of *Odo*MMSDH bound to NAD was prepared for modeling using the protein preparation wizard in Maestro v9.5 software (Schrödinger) by removing water molecules, assigning the bond order, and adding missing side chains and hydrogen atoms. The rotamer states of Asn and Gln and the charge states of His were also optimized. The thioacyl intermediate state was modeled by covalently linking MMSA to the sulfur atom of Cys280. Conformational scanning was conducted on thiohemiacetal intermediates using the MacroModel program (Schrödinger) to identify the low-energy conformation. The final model was minimized using Prime v3.1 (Schrödinger).

Results and Discussion

Overall structure of *Odo*MMSDH

*Odo*MMSDH (EC 1.2.1.27) is a key enzyme in the DMSP cleavage pathway and catalyzes the conversion of MMSA into propionyl-CoA using NAD and CoA as cofactors. Analytical size-exclusion chromatography experiments indicated that *Odo*MMSDH exists as a dimer in solution (Fig. 1). The crystal structure of *Odo*MMSDH, which was refined to 2.9 Å resolution, showed that the asymmetric unit is composed of six dimers. The overall root-mean-square deviations (RMSD) for the backbone atoms among the six dimers were all less than 0.65 Å, showing little structural variation among the dimers in the asymmetric unit. The dimer interface area between subunits A and B was 846.2 Å^2 for subunit A (approximately 14.1% of total area, 5999.3 Å^2) and 842.6 Å^2 for subunit B (approximately 14.5% of total area, 5807.5 Å^2) (Fig. 1).

The monomeric structure of *Odo*MMSDH is composed of 14 α-helices and 19 β-strands, which form an NAD-binding domain (α2–α7, α14, β1–β4, and β7–β11), a substrate-binding domain (α8–α13, β12–β18), and an oligomerization domain (β5, β6, and β19) (Fig. 2). The NAD-binding and substrate-binding domains showed an α/β structure similar to the Rossmann fold, with six central β-sheets surrounded by α-helices; α1, α4–α7, α14, and α9–α13, respec-

tively. The oligomerization domain is composed of three antiparallel strands (β5, β6, and β19). Each dimer is formed via hydrogen bonding interactions between β19 of subunit A and β18 of subunit B (Fig. 2).

Structure of NAD and the substrate-binding site

The first crystal structure of MMSDH from *Bacillus subtilis* (*Bsu*MMSDH) (approximately 43% sequence identity with *Odo*MMSDH) was determined to be a tetramer in the presence of an NAD cofactor (PDB code: 1T90) (Bchini *et al.*, 2012). The tetramer forms through dimer-dimer interactions. The dimer structures of *Bsu*MMSDH are very similar to the dimeric *Odo*MMSDH structure. The overall RMSD of the Cα atomic positions of the dimers was only 1.01 Å. When non-crystallographic two-fold symmetry is considered, the dimeric *Odo*MMSDH structure generated a tetramer very similar to that observed in *Bsu*MMSDH structures. Sequence alignment results as well as structural superposition showed that both NAD and the substrate-binding sites were highly conserved between the two proteins (Fig. 2). In addition, the MMSDH structures (*Sme*MMSDH) from *Sinorhizobium meliloti* were solved in complex with NAD (PDB code 4IYM) and without NAD (PDB code 4E4G). Both structures were annotated as tetramers without experimental support for the claim (Supplementary data Figs. S1 and S2). No report has been published describing the detailed structural features.

Tetrameric forms (Human ALDH2, Bovine ALDH2, and Cod ALDH9) (Steinmetz *et al.*, 1997; Johansson *et al.*, 1998; Ni *et al.*, 1999) and a dimeric form (Rat ALDH3) (Liu *et al.*, 1997) of ALDH have been reported, such as those observed for *Bsu*MMSDH (tetramer) (Bchini *et al.*, 2012), *Sme*MMSDH (tetramer; tentative), and *Odo*MMSDH (dimer). Interestingly, a moderate sequence similarity was found between MMSDHs and ALDHs (17 to 23% sequence identity). However, these two proteins share significant structural homology and oligomerization states such as homodimers or homotetramers (Supplementary data Fig. S3). In the BsuMMSDH structre, higher number of residues are involved in the dimer formation than the tetramer formation. Also, the dimer forming residues are better conserved when the sequence is aligned to all MMSDH enzymes with their structures disclosed (Fig. 2C). This suggests that the tetramer formation is non-essential for enzymatic catalysis of MMSDHs in general.

Of the 12 monomers of *Odo*MMSDH in the asymmetric unit, NAD molecule was modeled in six monomers with clear electron densities (subunits A, C, D, E, I, and L), whereas the remaining six subunits (B, F, G, H, J, and K) lacked sufficient electron density for acceptable placement of NAD. Furthermore, the occupancy refinements after placing NADs at these subunits showed the values to be close to zero, indicating that these sites were poorly occupied by NADs, or the NAD-unbound state. Structural superposition of the NAD-bound form (Subunit A) onto the NAD-unbound form (Subunit B) shows only small differences in relative side-chain orientations in Lsy172, Glu175, and Arg176 residues, while overall Cα positions overlap well (Fig. 3). This result is in line with the observation in *Sme*MMSDH structures where overlay of the two tetrameric states (NAD-bound and NAD-unbound) shows Cα RMSD of less than 0.4 Å, indicating no structural alteration upon NAD binding.
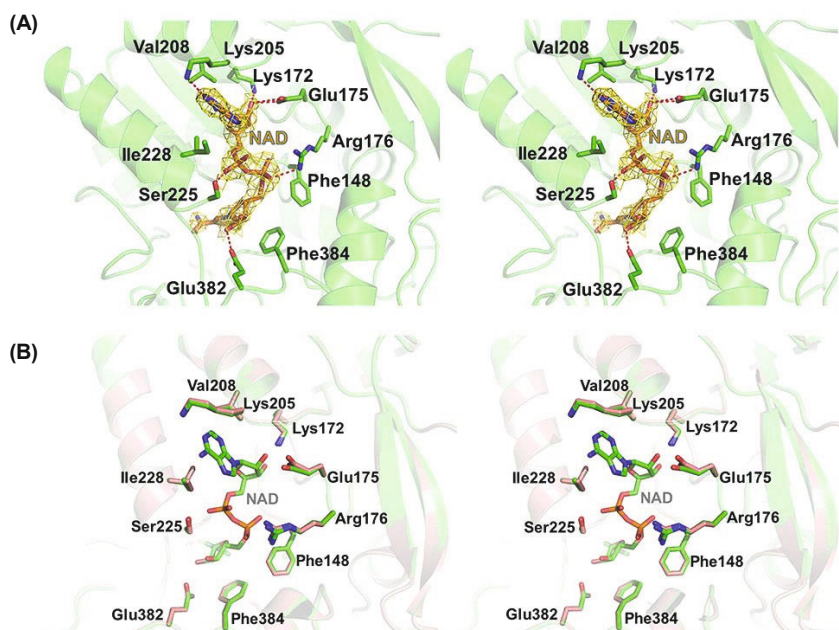
(A)

(B)

Fig. 3. Structure of the NAD-binding region in *Odo*MMSDH. (A) Stereoscopic representation showing the interactions between NAD and *Odo*MMSDH. Interacting residues are represented as green stick models. Bound NAD is shown as yellow-based stick models with a 2Fo-Fc electron density map (contoured at 1σ). Dotted lines designate hydrogen bonds. Residues without dotted lines have hydrophobic interactions with NAD. (B) Structural superposition of NAD-bound (Subunit A, green) and NAD-unbound (Subunit B, salmon) forms of the *Odo*MMSDH structure is shown in stereo view. The results show that the overall structure of the NAD-bound form is very similar to that of the NAD-unbound form, but there are small side-chain movements in the Lys172, Glu175, and Arg176 residues.

In the *Odo*MMSDH structure, the hydrophobic adenine ring of NAD was bound to the hydrophobic pocket formed by Val208 and Ile228. The adenine ribose oxygen forms hydrogen bonds with the side chains of Lys172. The phosphate group forms a hydrogen bond with the conserved Ser225. The nicotinamide ribose oxygen forms hydrogen bonds with the conserved Glu382 and backbone oxygen of Gly247. The nicotinamide ring forms extensive hydrophobic interactions with Pro147, Val154, Val223, and Gly224. Interestingly, Glu382 and Phe384 residues in the substrate-binding domain were also involved in the NAD interaction (Figs. 2 and 3). Diffused electron density for the nicotinamide of NAD in subunits A, I, and L indicates that the nicotinamide-protein interaction is relatively dynamic compared to the rest of the NAD-protein interactions. This was also observed as higher B-factors in the nicotinamide moiety of subunits A and C. Residues involved in NAD binding are highly conserved across all MMSDH enzymes and are structurally similar among all twelve subunits, with the exception of two residues, Arg176 and Lys205. Notably, the corresponding residues in other MMSDH structures showed conformational differences between the NAD-free and NAD-bound forms, indicating that NAD binding likely induced conformational changes in the side chains of these two residues (Fig. 3 and Supplementary data Fig. S2). Notably, Cys280, the catalytic residue used as a proton donor for the enzymatic reaction of *Odo*MMSDH, is in close proximity to the nicotinamide group with an average distance of 2.75 Å between the sulfur on cysteine to C4 of nicotinamide.

The NAD and the substrate-binding sites of *Odo*MMSDH are adjacent to one another. However, the entrances to these sites are in opposite locations (Fig. 4) and the two binding sites are segregated and bordered by residues Phe150, Met153, Val154, Trp 157, Cys280, Met281, and Phe449. The substrate pocket is surrounded by residues Arg103, Arg279, Leu440, and Val442. The bottom of this pocket is lined by a number of polar groups, including Asp90, Arg103, Ser275, and Arg-279. Basic residues in the cleft region (Arg103 and Arg279 in *Odo*MMSDH, and Arg107 and Arg283 in *Bsu*MMSDH) were predicted to anchor the C-1 carboxyl group (Fig. 4). Additional highly conserved residues found in the cleft region of *Odo*MMSDH included Arg64 and Arg66, corresponding to Arg68 and Arg70 of *Bsu*MMSDH, which form a basic binding pocket. Each substrate contains two possible negatively charged atoms, carbonate and aldehyde, which
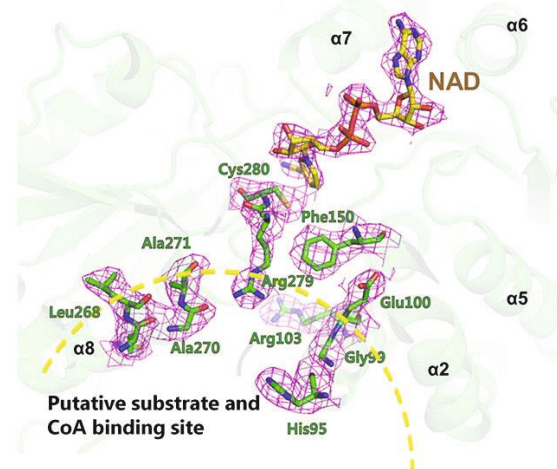

Fig. 4. Putative substrate- and CoA-binding site of *Odo*MMSDH. The bound NAD molecule is shown as yellow stick-based models, while the putative substrate-binding site is shown in a yellow dotted circle. The substrate-binding site has a relatively positive charge and originated from the Arg64, Arg66, Arg103, and Arg279 residues. Notably, Cys280 (catalytic residue) is closely located to the nicotinamide group of NAD. Electron density map around the putative substrate and CoA-binding site. 2Fo-Fc electron density at the substrate-binding site, including NAD, is indicated by magenta, contoured at 1σ.
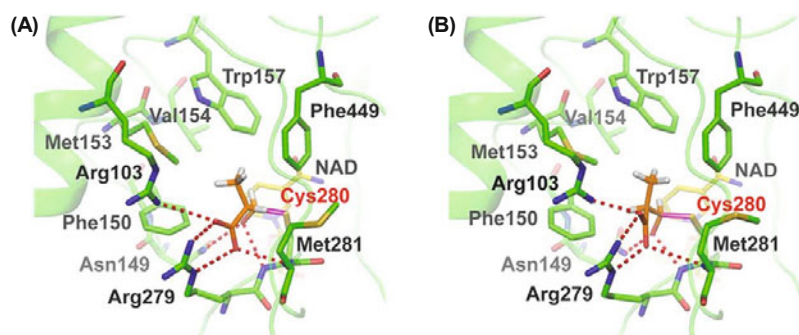
(A) **(B)**

Fig. 5. Computational models of the thiohemiacetal intermediate states of *Odo*MMSDH. The (*S*)- and (*R*)-thiohemiacetal intermediates that are shown as orange sticks in panels (A) and (B), respectively, are covalently bound to the sulfur atom of Cys280 (labeled in red). The stereochemical state of the intermediate has little impact on protein interaction. The residues involved in substrate binding are shown as green sticks with their labeled residue numbers. The covalent bond between the thiohemiacetal intermediate and Cys280 is colored magenta. NAD is colored in yellow. Hydrogen bonds are represented as red dashed lines.

may interact with the binding pocket. Sequence alignment among ALDHs indicated that the Arg103 and Arg279 residues of *Odo*MMSDH were absent in the betaine aldehyde dehydrogenase from cod liver (PDB code: 1A4S) (Johansson *et al.*, 1998), suggesting that the carboxyl group of the substrate is essential for its approach to the enzyme. Additionally, the enzymatic reaction was conducted in the center of a narrow funnel between the pockets. In the dual binding mode, substrates can approach the active site for decarboxylation with a higher affinity (Talfournier *et al.*, 2011).

Computational modeling of a thioacyl intermediate for Cys280 of *Odo*MMSDH

The substrate of *Odo*MMSDH produces a short-lived intermediate that is quickly converted into a hydrogen carbonate ion and propionyl-CoA. Thus, it is very difficult to obtain a crystal structure of *Odo*MMSDH in complex with its substrate. To overcome this limitation and gain insight into the interactions between *Odo*MMSDH and its substrate, we employed computational modeling of the intermediate states of the enzyme reaction. Based on previous biochemical and structural studies of other ALDHs, the enantiomeric tetrahedral intermediates of *Odo*MMSDH were modeled using the NAD-bound crystal structure. Briefly, a tetrahedral intermediate of MMSA was modeled to the sulfur cysteine side chain of Cys280. The covalent adduct was subjected to quick energy minimization followed by conformational searching to further identify the lowest energy conformation. Finally, the lowest energy conformation of the model was energy-minimized for atoms within a 4 Å radius of the covalently modified Cys280 (Fig. 5).

The minimized structures showed that the hydrogen atoms of thiohemiacetal in both stereoisomers point towards the C-4 position of the nicotinamide ring. The substrate-binding pocket of *Odo*MMSDH is constructed by conserved basic residues (Arg103 and Arg279) and hydrophobic residues (Phe150, Met153, Val154, Trp 157, Met281, and Phe449). The propyl group of the intermediate is sandwiched between Phe150 and Met281, while the methyl group is nested in a hydrophobic pocket constructed by Met153, Trp157, and Phe449. The latter two residues also participate in the formation of the nicotinamide ring-binding pocket of the NAD binding site (Fig. 5).

In a previous study by Talfournier *et al.* (2011), substitution of Arg124 and Arg301 for Leu residues in *Bsu*MMSDH decreased the second-order rate constant k_2 by 55 and 62-

fold in the pre-steady-state condition, indicating involvement of these residues in proper positioning and stabilization of the substrate. In the model structure, the carboxylate anion of thiopropyl interacts with both Arg103 and Arg279 through salt bridges. It is likely that this interaction is preserved throughout the enzyme reaction until the β-decarboxylation step in order to stabilize the substrate. The oxyanion of the tetrahedral intermediate was within H-bonding distance of the backbone and side chain amine groups of Cys280 and Asn149, indicating that these two amine groups serve as the oxyanion hole. Qualitatively, both R- and S-stereoisomer showed little difference in binding modes, indicating no discrimination of the isomers.

In summary, we determined the structure of *Odo*MMSDH in the presence of an NAD cofactor and compared it with the previously described structures (Talfournier *et al.*, 2011; Bchini *et al.*, 2012). Furthermore, we propose an MMSA binding mode by *Odo*MMSDH based on the crystal structure of *Odo*MMSDH and *in silico* modeling. The model structures enabled identification of key residues responsible for MMSA binding and enzyme reactions as well as reaction intermediate stabilization in *Odo*MMSDH.

References

Adams, P.D., Grosse-Kunstleve, R.W., Hung, L.W., Ioerger, T.R., McCoy, A.J., Moriarty, N.W., Read, R.J., Sacchettini, J.C., Sauter, N.K., and Terwilliger, T.C. 2002. PHENIX: building new software for automated crystallographic structure determination. *Acta Crystallogr. D Biol. Crystallogr.* **58**, 1948–1954.

Bannerjee, D., Sanders, L.E., and Sokatch, J.R. 1970. Properties of purified methylmalonate semialdehyde dehydrogenase of *Pseudomonas aeruginosa*. *J. Biol. Chem.* **245**, 1828–1835.

Battye, T.G.G., Kontogiannis, L., Johnson, O., Powell, H.R., and Leslie, A.G. 2011. iMOSFLM: a new graphical interface for diffraction-image processing with MOSFLM. *Acta Crystallogr. D Biol. Crystallogr.* **67**, 271–281.

Bchini, R., Dubourg-Gerecke, H., Rahuel-Clermont, S., Aubry, A.,

Branlant, G., Didierjean, C., and Talfournier, F. 2012. Adenine binding mode is a key factor in triggering the early release of NADH in coenzyme A-dependent methylmalonate semialdehyde dehydrogenase. *J. Biol. Chem.* **287**, 31095–31103.

Chen, V.B., Arendall, W.B., Headd, J.J., Keedy, D.A., Immormino, R.M., Kapral, G.J., Murray, L.W., Richardson, J.S., and Richardson, D.C. 2009. MolProbity: all-atom structure validation for macromolecular crystallography. *Acta Crystallogr. D Biol. Crystallogr.* **66**, 12–21.

Curson, A.R., Fowler, E.K., Dickens, S., Johnston, A.W., and Todd, J.D. 2012. Multiple DMSP lyases in the γ-proteobacterium *Oceanimonas doudoroffii*. *Biogeochemistry* **110**, 109–119.

Curson, A.R., Sullivan, M.J., Todd, J.D., and Johnston, A.W. 2011a. DddY, a periplasmic dimethylsulfoniopropionate lyase found in taxonomically diverse species of Proteobacteria. *ISME J.* **5**, 1191–1200.

Curson, A.R., Todd, J.D., Sullivan, M.J., and Johnston, A.W. 2011b. Catabolism of dimethylsulphoniopropionate: microorganisms, enzymes and genes. *Nat. Rev. Microbiol.* **9**, 849–859.

Emsley, P. and Cowtan, K. 2004. Coot: model-building tools for molecular graphics. *Acta Crystallogr. D Biol. Crystallogr.* **60**, 2126–2132.

Hempel, J., Nicholas, H., and Lindahl, R. 1993. Aldehyde dehydrogenases: widespread structural and functional diversity within a shared framework. *Protein Sci.* **2**, 1890–1900.

Johansson, K., Ramaswamy, S., Eklund, H., El-Ahmad, M., Hjelmqvist, L., and Jörnvall, H. 1998. Structure of betaine aldehyde dehydrogenase at 2.1 Å resolution. *Protein Sci.* **7**, 2106–2117.

Laskowski, R.A., MacArthur, M.W., Moss, D.S., and Thornton, J.M. 1993. PROCHECK: a program to check the stereochemical quality of protein structures. *J. Appl. Crystallogr.* **26**, 283–291.

Liu, Z.J., Sun, Y.J., Rose, J., Chung, Y.J., Hsiao, C.D., Chang, W.R., Kuo, I., Perozich, J., Lindahl, R., and Hempel, J. 1997. The first structure of an aldehyde dehydrogenase reveals novel interactions between NAD and the Rossmann fold. *Nat. Struc. Mol. Biol.* **4**, 317–326.

Murshudov, G.N., Skubák, P., Lebedev, A.A., Pannu, N.S., Steiner, R.A., Nicholls, R.A., Winn, M.D., Long, F., and Vagin, A.A. 2011. REFMAC5 for the refinement of macromolecular crystal structures. *Acta Crystallogr. D Biol. Crystallogr.* **67**, 355–367.

Ni, L., Zhou, J., Hurley, T.D., and Weiner, H. 1999. Human liver mitochondrial aldehyde dehydrogenase: three-dimensional structure and the restoration of solubility and activity of chimeric forms. *Protein Sci.* **8**, 2784–2790.

Nwachukwu, J.C., Southern, M.R., Kiefer, J.R., Afonine, P.V., Adams, P.D., Terwilliger, T.C., and Nettles, K.W. 2013. Improved crystallographic structures using extensive combinatorial refinement. *Structure* **21**, 1923–1930.

Reisch, C.R., Moran, M.A., and Whitman, W.B. 2011. Bacterial catabolism of dimethylsulfoniopropionate (DMSP). *Front. Microbiol.* **2**, 172.

Steele, M., Lorenz, D., Hatter, K., Park, A., and Sokatch, J. 1992. Characterization of the mmsAB operon of *Pseudomonas aeruginosa* PAO encoding methylmalonate-semialdehyde dehydrogenase and 3-hydroxyisobutyrate dehydrogenase. *J. Biol. Chem.* **267**, 13585–13592.

Stefels, J. 2000. Physiological aspects of the production and conversion of DMSP in marine algae and higher plants. *J. Sea Res.* **43**, 183–197.

Steinmetz, C.G., Xie, P., Weiner, H., and Hurley, T.D. 1997. Structure of mitochondrial aldehyde dehydrogenase: the genetic component of ethanol aversion. *Structure* **5**, 701–711.

Stines-Chaumeil, C., Talfournier, F., and Branlant, G. 2006. Mechanistic characterization of the MSDH (methylmalonate semialdehyde dehydrogenase) from *Bacillus subtilis*. *Biochem. J.* **395**, 107–115.

Sunda, W., Kieber, D., Kiene, R., and Huntsman, S. 2002. An antioxidant function for DMSP and DMS in marine algae. *Nature* **418**, 317–320.

Talfournier, F., Stines-Chaumeil, C., and Branlant, G. 2011. Methylmalonate-semialdehyde dehydrogenase from *Bacillus subtilis* substrate specificity and coenzyme A binding. *J. Biol. Chem.* **286**, 21971–21981.

Todd, J.D., Curson, A.R., Kirkwood, M., Sullivan, M.J., Green, R.T., and Johnston, A.W. 2011. DddQ, a novel, cupin-containing, dimethylsulfoniopropionate lyase in marine roseobacters and in uncultured marine bacteria. *Environ. Microbiol.* **13**, 427–438.

Todd, J.D., Curson, A.R., Nikolaidou-Katsaraidou, N., Brearley, C.A., Watmough, N.J., Chan, Y., Page, P.C., Sun, L., and Johnston, A.W. 2010. Molecular dissection of bacterial acrylate catabolism–unexpected links with dimethylsulfoniopropionate catabolism and dimethyl sulfide production. *Environ. Microbiol.* **12**, 327–343.

Todd, J.D., Kirkwood, M., Newton-Payne, S., and Johnston, A.W. 2012. DddW, a third DMSP lyase in a model Roseobacter marine bacterium, *Ruegeria pomeroyi* DSS-3. *ISME J.* **6**, 223–226.

Vagin, A. and Teplyakov, A. 1997. MOLREP: an automated program for molecular replacement. *J. Appl. Crystallog.* **30**, 1022–1025.

Vasiliou, V. and Nebert, D.W. 2005. Analysis and update of the human aldehyde dehydrogenase (ALDH) gene family. *Hum. Genomics* **2**, 138.

Winn, M.D., Ballard, C.C., Cowtan, K.D., Dodson, E.J., Emsley, P., Evans, P.R., Keegan, R.M., Krissinel, E.B., Leslie, A.G., and McCoy, A. 2011. Overview of the CCP4 suite and current developments. *Acta Crystallogr. D Biol. Crystallogr.* **67**, 235–242.

Zhang, Y.X., Tang, L., and Hutchinson, C.R. 1996. Cloning and characterization of a gene (*msdA*) encoding methylmalonic acid semialdehyde dehydrogenase from *Streptomyces coelicolor*. *J. Bacteriol.* **178**, 490–495.